DYNAMIC FRACTURE OF THIN STRUCTURES

V. Gupta

IIT Delhi, India

ABSTRACT

A meshless shell method for dynamic fracture problems based on normalized Smoothed Particle Hydrodynamics (SPH) is presented. The SPH method is corrected by a normalization in order to fulfill completeness requirement. Instability are controlled by stress-point integration. The method is modified for Mindlin-Reissner shell analysis. Stress based fracture criterion is incorporated based on the visibility method. The method is applied to two dynamic fracture problems in thin-walled pipes including fluid-structure interaction. The results are compared to experimental data and they are very promising.

Key words: shell, fracture, SPH.

1. INTRODUCTION

The simulation of complex fracture-phenomena of thin-walled structures using traditional tools such as the finite element method is extremely difficult. Large deformations and the cracking of solids [VE99, OR99, JVC04, VE06] are complex and costly to model with classical numerical methods that are based on meshes. Therefore, so-called meshless methods have been developed that are well-suited to model problems involving large deformations, fracture and other complex problems that could for example involve the interaction between a fluid and a structure [FB07, RB04, BLG95, BT96].

One of the most efficient meshless method is the Smoothed Particle Hydrodynamics (SPH) method [GM77]. In contrast to many other weak-formulation based meshless methods, SPH is a collocation method based on the strong formulation of the problem. The advantage of high computational efficiency unfortunately comes at cost of two major drawbacks:

- Numerical Instabilities
- Insufficient polynomial order of completeness

Numerical instabilities occur due to under-integration. These instabilities were discussed extensively in the SPH literature [VCL00, SHA95, RL00, RPB05, CWYY01, WC06] and techniques such as stress point integration eliminate or at least attenuate these instabilities. The insufficient order of completeness is attributed to the SPH formulation itself. The classical SPH formulation is not able to reproduce even a constant function exactly. Therefore, procedures have been developed that correct the SPH formulation in a way constant and linear functions can be reproduced exactly [RL97, KHG08, BK00, LJZ95, BKO$^+$96, KB97, JB96].

The SPH method is a continuum based method. However, in the case of thin structures, three-dimensional continuum formulation becomes computationally inefficient. Therefore, the possibility to model these structures with a single layer of nodes is very attractive. Meshless shell methods already exist [KB96, NKM00, RAB07, RA06, Lei01, LC04] but they are all based on weak formulations and therefore computationally expensive. Moreover, most of these methods do not account for fracture of the shell.

In this paper, we present an SPH shell method for dynamic elastoplastic fracture problems. The most pertinent feature of our new formulation is its simplicity and computational efficiency. We firstly present classical SPH formulation and corrected SPH formulation that guarantees first-order completeness, i.e. the ability to reproduce linear functions. Secondly, the corrected SPH formulation is extended to model shell-structures. Finally, the elasto-plastic constitutive model and fracture criteria are presented before two examples demonstrate the capability of our method.

2. NORMALIZED SMOOTHED PARTICLE HYDRODYNAMICS (NSPH)

The SPH formulation is based on a representation of the field through a set of particles given by

$$\mathbf{u}_I = \sum_{J=1}^{N} N_{IJ}\mathbf{u}_J \tag{1}$$

where $\mathbf{u}_I$ is the node of interest, $\mathbf{u}_J$ are neighboring nodal parameters, N is the number of neighboring particles for which the SPH shape functions N_{IJ} are unequal to zero. In the classical SPH theory, N_{IJ} is calculated

Proc. '5th European Conference on Space Debris', Darmstadt, Germany 30 March – 2 April 2009, (ESA SP-672, July 2009)

from the SPH kernel function $W(r_{IJ}, h)$:

$$N_{IJ} = V_J \, W(r_{IJ}, h_{IJ}) \tag{2}$$

where r_{IJ} represents the distance between particles I and J, V_J is the volume associated with particle J and h_{IJ} is the averaged smoothing length between particles I and J, that determines the size of the support domain. The kernel function and hence also the shape functions do commonly have compact support, meaning they are unequal to zero in a certain neighborhood and equalize zero behind this neighborhood. A common kernel function is the B-spline:

$$W(r_{IJ}, h) \quad = \quad W(s) = \begin{cases} 1 - 6s^2 + 8s^3 - 3s^4 & s \leq 1 \\ 0 & s > 1 \end{cases} \quad , \quad s = \frac{\mathbf{X}_J - \mathbf{X}_I}{2h} \tag{3}$$

that has circular support size determined by the smoothing length h. Gradients of functions in SPH formulation is approximated by

$$\nabla \mathbf{u}_I = \sum_{J=1}^{N} \nabla N_{IJ} \otimes (\mathbf{u}_J - \mathbf{u}_I) \tag{4}$$

The second term in the brackets is added to ensure that SPH fulfills at least zero-order completeness. That zero-order completeness is violated can easily be observed by considering the derivatives of the constant function, e.g. 1, that cannot be reproduced, i.e. $\nabla 1 = \sum_{J=1}^{N} \nabla N_{IJ} \neq \mathbf{0}$. First-order completeness is not achieved in classical SPH. This means that gradient of a constant field cannot be enforced at the boundaries of the volume and that linear strain fields cannot be reproduced exactly. The corrected SPH formulation we adopted is based on normalization of derivatives of the shape functions [RL00], therefore called NSPH subsequently. NSPH modifies eq. (4) with correction matrix $\mathbf{B}$:

$$\nabla \mathbf{u}_I \quad = \quad \sum_{J=1}^{N} \nabla N_{IJ} \otimes (\mathbf{u}_J - \mathbf{u}_I) \cdot \mathbf{B} \tag{5}$$

$$\mathbf{B} \quad = \quad \mathbf{H}^{-1} \tag{6}$$

$$\mathbf{H} \quad = \quad \sum_{J=1}^{N} (\mathbf{X}_J - \mathbf{X}_I) \otimes \nabla N_{IJ} \tag{7}$$

that is constructed in a way eq. (5) fulfills first-order completeness. Defining

$$\nabla \hat{N}_{IJ} = \nabla N_{IJ} \cdot \mathbf{B} \tag{8}$$

we can rewrite eq. (5)

$$\nabla \mathbf{u}_I \quad = \quad \sum_{J=1}^{N} \nabla \hat{N}_{IJ} \otimes (\mathbf{u}_J - \mathbf{u}_I) \tag{9}$$

The conservation of linear momentum in the absence of body forces is given by

$$\varrho \ddot{\mathbf{u}} = \nabla \mathbf{P} \tag{10}$$

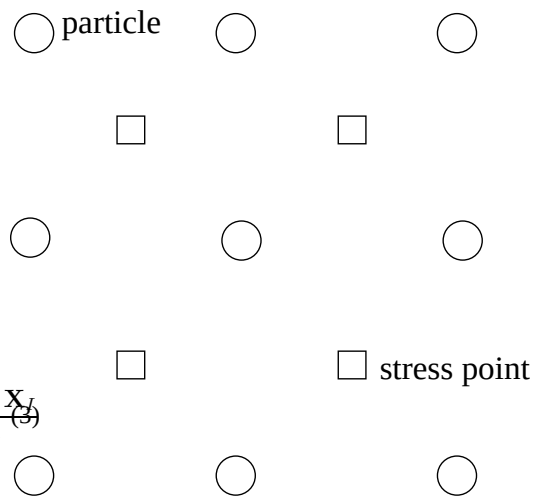

Figure 1. Stress points are added in order to avoid instabilities

and in NSPH formalism by

$$\varrho \ddot{\mathbf{u}}_I = \sum_{J=1}^{N} (\mathbf{P}_J - \mathbf{P}_I) \, \nabla \hat{N}_{IJ} \tag{11}$$

We use Total Lagrangian formulation instead of updated Lagrangian formulation used in early SPH-formulation since recent studies have shown that certain numerical instabilities can be related to the use of Eulerian kernels expressed in spatial coordinates instead of material coordinates. It was also demonstrated that these instabilities can be avoided by using Lagrangian kernels expressed in material coordinates [RBX04]. This is especially important for fracture. One would like to avoid spurious material fracture that often occurs when Eulerian kernels are employed.

Numerical instabilities due to under-integration are eliminated by introducing stress-points. Stresses are evaluated at stress points instead of the collocation points leading to the following equation:

$$\varrho \ddot{\mathbf{u}}_I = \sum_{K=1}^{N_S} (\mathbf{P}_K - \mathbf{P}_I) \, \nabla \hat{N}_{IJ} \tag{12}$$

where N_S is the set of stress points. Stress points are added into the structured discretization as illustrated in figure 1.

3. NSPH SHELL FORMULATION

In this section, we extend the continuum NSPH-formulation to MindlinReissner shell NSPH formulation. Therefore, the behavior of the shell is determined using a model discretized only on mean surface alone that consists of a single layer of particles. Each point on the mean

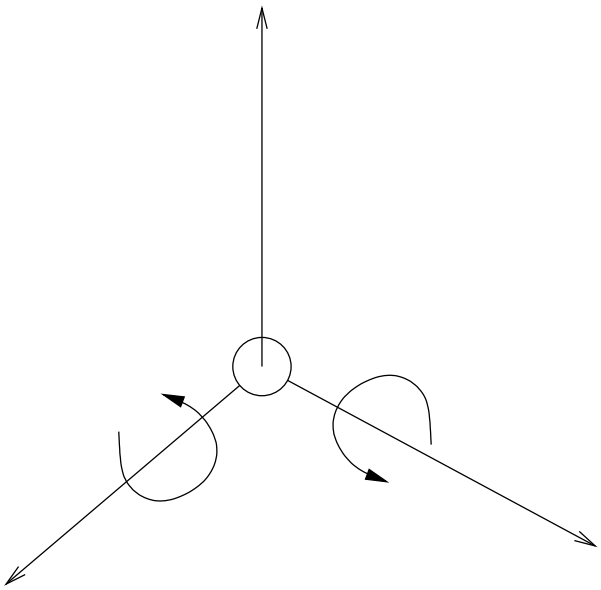

Figure 2. SPH shell particle

plane is assigned a thickness that varies in space and time. Each particle has five degrees of freedom (DOF): three translational DOFs and two rotational DOFs lying in the plane tangent to the shell, figure 2. Particles have no degree of freedom perpendicular to the plane, i.e. no drilling rotation. The position vector in the initial configuration $\mathbf{X}$ of any point M located at a distance ξ from the mean plane can be expressed as

$$\mathbf{X} = \mathbf{X}_M + \xi \mathbf{n} \tag{13}$$

with $\xi \in [-0.5t, 0.5t]$, t being the thickness of the shell, $\mathbf{n}$ is the pseudo-normal vector that represents the orientation of the material with respect to the mean plane and $\mathbf{X}_M$ being points on the mean surface. Similarly, we obtain the displacement vector

$$\mathbf{u} = \mathbf{u}_M + \xi \left(\mathbf{n} - \mathbf{n}_0\right) \tag{14}$$

with $\mathbf{n}_0$ being the pseudo-normal vector in the initial configuration. The technique for updating $\mathbf{n}$ will be described later.

Firstly, we define the local coordinate system associated with the shell in the initial configuration that is denoted by L_0 subsequently. The initial local coordinates $\mathbf{x}_{L_0}$ of each point are defined from the general initial coordinates $\mathbf{x}_0$ through a rotation matrix

$$\mathbf{x}_0 = \mathbf{G}_0^{-1} \cdot \mathbf{x}_{L_0} \tag{15}$$

With these definitions, the displacement vector in eq. (14) can be rewritten as

$$\mathbf{u}(x_{L_0}, y_{L_0}) = \mathbf{u}_M(x_{L_0}, y_{L_0}) + z_{L_0} \left(\mathbf{n}(x_{L_0}, y_{L_0}) - \mathbf{n}_0(x_{L_0}, y_{L_0})\right) \tag{16}$$

Since fibers are initially perpendicular to the mean plane of the shell, $\mathbf{n}_0$ is parallel to the z_{L_0} axis, which implies that $z_{L_0} = \xi$. Then, in L_0 , one calculates the total Lagrangian NSPH shape functions N_{L_0} leading to the expression of the gradient of a field in the global coordinate system L_G:

$$\nabla u = \mathbf{G}_0 \cdot \nabla_{L_0} u \tag{17}$$

Now, one can define the gradient matrix $\mathbf{F}$ for a point on the mean plane ($z_{L_0} = \xi = 0$):

$$\mathbf{F} = \mathbf{G}_0 \cdot \mathbf{F}_3 \tag{18}$$

with

$$\mathbf{F}_3 = \begin{bmatrix} x_{,x_{L_0}} & x_{,y_{L_0}} & n_x \\ y_{,x_{L_0}} & y_{,y_{L_0}} & n_y \\ z_{,x_{L_0}} & z_{,y_{L_0}} & n_z \end{bmatrix} \tag{19}$$

We now express the Green-Lagrange strain tensor:

$$E_{ij} = 0.5 \left(u_{i,j} + u_{j,i}\right) = E_{Mij} + E_{Bij}(\xi) \tag{20}$$

with

$$E_{Mij} = 0.5 \left(u_{Mi,j} + u_{Mj,i}\right) \tag{21}$$

and

$$E_{Bij}(\xi) = \frac{\xi}{2} \left(\Delta n_{i,j} + \Delta n_{j,i}\right) \tag{22}$$

with $\Delta \mathbf{n} = \mathbf{n} - \mathbf{n}_0$. As indicated by above equations, $\mathbf{E}$ is divided into a part $\mathbf{E}_M$ which is constant throughout the thickness, associated with membrane and transverse shear effects, and a part $\mathbf{E}_B(\xi)$ which is linear throughout the thickness, associated with bending effects. For geometrical non-linear applications (especially for large rotations), the usual non-linear membrane strains are added to the linear membrane ones. The non-linear bending and shear strains are neglected as usual for non-linear shell formulations. Then, strains must be written in the local coordinate system of the current position of the mean plane of the plate, denoted by L_C , in order to calculate the stresses in agreement with the plane stress assumption. In order to define this coordinate system, one determines two vectors $\mathbf{n}_2'$ and $\mathbf{n}_2$ of the mean plane. The normal to the plane is defined by

$$\mathbf{n}_2' = \frac{\partial \mathbf{X}(x_L, y_L)}{\partial x_L} \tag{23}$$

$$\mathbf{n}_2 = \frac{\partial \mathbf{X}(x_L, y_L)}{\partial y_L} \tag{24}$$

$$\mathbf{n}_3 = \mathbf{n}_2' \wedge \mathbf{n}_2 \tag{25}$$

The basis is completed with a third vector:

$$\mathbf{n}_1 = \mathbf{n}_3 \wedge \mathbf{n}_2 \tag{26}$$

Using these three basis vectors, the rotation matrix $\mathbf{G}_L$ is defined that connects the current local system L_C to the global system L_G. One should note that in the case

of an updated Lagrangian formulation in which the reference configuration is regularly updated the equality $\mathbf{G}_0 = \mathbf{G}_L$ holds. The expression of the local membrane shear strains ϵ_{L_M} and bending strains ϵ_{L_B} follows

$$\begin{aligned} \epsilon_{L_M} &= \mathbf{G}_L \cdot \mathbf{F}^{-t} \cdot \mathbf{E}_M \cdot \mathbf{F}^{-1} \cdot \mathbf{G}_L^T \quad (27) \\ \epsilon_{L_B} &= \mathbf{G}_L \cdot \mathbf{F}^{-t} \cdot \mathbf{E}_B \cdot \mathbf{F}^{-1} \cdot \mathbf{G}_L^T \quad (28) \end{aligned}$$

which can be rewritten, still in the L_C coordinate system, in the form of generalized strain vectors ϵ_g and ϵ_s defined by:

$$\epsilon_g = \begin{pmatrix} \epsilon_{L_{m_{xx}}} \\ \epsilon_{L_{m_{yy}}} \\ \epsilon_{L_{m_{xy}}} \\ \epsilon_{L_{f_{xx}}} \\ \epsilon_{L_{f_{yy}}} \\ \epsilon_{L_{f_{xy}}} \end{pmatrix} \ , \ \epsilon_s = \begin{pmatrix} \epsilon_{L_{s_{xz}}} \\ \epsilon_{L_{s_{yz}}} \\ 0 \end{pmatrix} \quad (29)$$

The generalized stress vectors σ_g and σ_s are obtained accordingly. The membrane and shear stress resultants N_{ij} and S_i along with the bending moments m_{ij} are obtained by integration through the thickness:

$$\begin{aligned} N_{ij} &= \int_{-h/2}^{h/2} \sigma_{L_{m_{ij}}}(\xi)\, d\xi = h\sigma_{L_{m_{ij}}} \\ S_i &= \int_{-h/2}^{h/2} \sigma_{L_{s_{iz}}}(\xi)\, d\xi = h\sigma_{L_{s_{iz}}} \\ m_{ij} &= \int_{-h/2}^{h/2} \sigma_{L_{b_{ij}}}(\xi) \cdot \xi \, d\xi = \frac{h^3}{12}\sigma_{L_{f_{bij}}} \quad (30) \end{aligned}$$

Hookes law in plane stress is used to link stresses to strains, and the transverse shear stresses are connected to the corresponding strains through the usual relations:

$$\sigma_{\mathbf{g}} = \mathbf{C} \cdot \epsilon_{\mathbf{g}} \ , \ \sigma_{\mathbf{s}} = G \cdot \epsilon_{\mathbf{s}} \quad (31)$$

where G is the shear modulus and with

$$\mathbf{C} = \begin{bmatrix} \hat{\mathbf{C}} & 0 \\ 0 & \hat{\mathbf{C}} \end{bmatrix} \quad (32)$$

where $\hat{\mathbf{C}}$ is the first-order elasticity tensor for plane stress conditions. Then, the generalized stresses integrated through the thickness are rewritten in the form of two matrices:

$$\mathbf{S} = \begin{bmatrix} N_{xx} & N_{xy} & T_x \\ N_{xy} & N_{yy} & T_y \\ T_x & T_y & 0 \end{bmatrix} \ , \ \mathbf{m} = \begin{bmatrix} m_{xx} & m_{xy} & 0 \\ m_{xy} & m_{yy} & 0 \\ 0 & 0 & 0 \end{bmatrix} \quad (33)$$

The nominal stress tensor $\mathbf{P}$ can then be obtained from

$$\mathbf{P} = \mathbf{G}_L^T \cdot \mathbf{S} \cdot \mathbf{G}_L \cdot \mathbf{F}^T = \mathbf{s} \cdot \mathbf{F}^T \quad (34)$$

Similar to the 3D case, the membrane and transverse shear equilibrium equation follows

$$\mathbf{P}^T \cdot \nabla = \varrho \cdot \ddot{\mathbf{u}} \quad (35)$$

Next, the angular accelerations $\ddot{\theta}_{x_L}$ and $\ddot{\theta}_{y_L}$ are calculated using the two moment equilibrium equations defined in the local coordinate system by

$$\begin{aligned} I \cdot \ddot{\theta}_{x_L} &= m_{yy,y} + m_{xy,x} + t \cdot \sigma_{yz} \\ I \cdot \ddot{\theta}_{y_L} &= m_{xx,x} + m_{xy,y} - t \cdot \sigma_{xz} \quad (36) \end{aligned}$$

or in matrix form

$$I \cdot \ddot{\theta}_L = \mathbf{L} \cdot div(\mathbf{m}) + \mathbf{T}_L = \mathbf{L} \cdot \mathbf{m}^T \cdot \nabla_L + \mathbf{T}_L \quad (37)$$

with the rotation moment of inertia I and

$$\mathbf{L} = \begin{bmatrix} 0 & 1 & 0 \\ 1 & 0 & 0 \\ 0 & 0 & 0 \end{bmatrix} \ , \ \mathbf{T}_L = \begin{bmatrix} h \cdot \sigma_{yz} \\ -h \cdot \sigma_{xz} \\ 0 \end{bmatrix} \quad (38)$$

Eq. (37) can be also obtained in the L_G coordinate system by

$$I_0 \cdot \ddot{\theta} = \mathbf{M}^T \cdot \nabla_0 + \mathbf{T}_0 \quad (39)$$

with

$$\mathbf{M} = J \cdot \mathbf{F}^{-1} \cdot \mathbf{G}_L^T \cdot \mathbf{m} \cdot \mathbf{L}^T \cdot \mathbf{G}_L \ , \ \mathbf{T}_0 = J \cdot \mathbf{G}_L \cdot \mathbf{T}_L \quad (40)$$

Thus, $\mathbf{M}$ is the equivalent for the bending stresses of the nominal stress tensor $\mathbf{P}$ for the stresses that are constant throughout the thickness. Following the total Lagrangian formalism, one obtains the following pair of equations:

$$\begin{aligned} I_0 \cdot \ddot{\theta} &= \sum_{J=1}^{N} (\mathbf{M}_J - \mathbf{M}_I) \nabla N_{0IJ} + \mathbf{T}_0 \\ \varrho \cdot \ddot{\mathbf{u}} &= (\mathbf{P}_J - \mathbf{P}_I) \nabla N_{0IJ} \quad (41) \end{aligned}$$

The vector of angular accelerations $\ddot{\theta}$ thus obtained is used to update $\mathbf{n}$. One defines a new matrix $\mathbf{G}_n^t$ that expresses the rotation of $\mathbf{n}$ with respect to its initial position $\mathbf{n}_0$, and whose increment $\Delta\mathbf{G}_n$ expresses the rotation of $\mathbf{n}$ during a time step. Using θ, one determines the incremental rotation vector $\Delta\theta$ that defines the rotation of $\mathbf{n}$ during a time step, thanks to time integration. The corresponding rotation matrix $\Delta\mathbf{G}_n$ is then calculated using the Rodrigues formula:

$$\begin{aligned} \mathbf{G}_n^{t+\Delta t} &= \Delta\mathbf{G}_n \cdot \mathbf{G}_n^t \\ \mathbf{n}^{t+\Delta t} &= \mathbf{G}_n^{t+\Delta t} \cdot \mathbf{n}_0 \quad (42) \end{aligned}$$

4. ELASTO-PLASTIC CONSTITUTIVE MODEL AND FRACTURE CRITERION

For elasto-plastic material, MindlinReissner assumption that the stresses vary linearly throughout the thickness is no longer valid. Therefore, stresses have to be integrated through the thickness. One of the most usual techniques in shell applications of the finite element method consists in performing the integration using a number of additional Gauss points distributed throughout the thickness. A simpler and less expensive method enables the

direct calculation of the plastic stresses from the membrane and bending generalized stresses. This approach is based on the assumption that the whole section becomes plastic at once: this assumption is true when the shell is subject to membrane loads alone. Thus, in the case of a perfectly plastic material, one can express the plasticity criterion as follows:

$$f = \sigma_{VM}^2 - \sigma_{Y0}^2 \tag{43}$$

with the equivalent stress

$$\sigma_{VM}^2 = \sigma_{Lm,eq}^2 + \frac{1}{\Psi^2}\sigma_{Lb,eq}^2 + \frac{1}{3\Psi}\sigma_{Lb,eq}\,\sigma_{Lb,eq} + \kappa\sigma_{Ls,eq}^2 \tag{44}$$

Similarly, the equivalent generalized stresses are given by

$$\begin{aligned}
\sigma_{Lm,eq}^2 &= \sigma_{Lm_{xx}}^2 + \sigma_{Lm_{yy}}^2 + 3\sigma_{Lm_{xy}}^2 - \sigma_{Lm_{xx}}\,\sigma_{Lm_{yy}} \\
\sigma_{Lb,eq}^2 &= \sigma_{Lb_{xx}}^2 + \sigma_{Lb_{yy}}^2 + 3\sigma_{Lb_{xy}}^2 - \sigma_{Lb_{xx}}\,\sigma_{Lb_{yy}} \\
\sigma_{Lm,eq}\sigma_{Lb,eq} &= \sigma_{Lm_{xx}}\,\sigma_{Lb_{xx}} + \sigma_{Lm_{yy}}\sigma_{Lb_{yy}} + 3\sigma_{Lm_{xy}}\,\sigma_{Lb_{xy}} \\
&- 0.5\left(\sigma_{Lm_{xx}}\,\sigma_{Lb_{yy}} + \sigma_{Lm_{yy}}\,\sigma_{Lb_{xx}}\right) \\
\sigma_{Ls,eq}^2 &= 3\sigma_{Ls_{xz}}^2 + 3\sigma_{Ls_{yz}}^2
\end{aligned} \tag{45}$$

Let us assume that transverse shear stresses are not involved in plasticity, which is equivalent to setting the parameter κ equal to zero. The parameter Ψ can be used to adjust the occurrence of the plastic hinge through the thickness. In the case of pure bending loading, $\Psi = 1$ means that a plastic hinge occurs as soon as the skin becomes plastic, and $\Psi = 1.5$ means that the plastic hinge occurs only once the whole thickness of the shell has become plastic. For a shell in pure bending, the moment/curvature law reveals an apparent strain hardening effect due to the progressive development of plasticity through the thickness. To take this effect into account, Crisfield modified eq. (44) by allowing the parameter Ψ to vary between 1 and 1.5 depending on the equivalent plastic strain in bending. Eq. (43) can then be easily extended to the case of materials with isotropic strain hardening by taking into account the strain hardening of the materials traction curve as a function of the equivalent plastic strain ϵ_p:

$$f = \sigma_{VM}^2 - \sigma_Y(\epsilon_p)^2 = \sigma_g^t \cdot \mathbf{H} \cdot \sigma_g - \sigma_Y(\epsilon_p)^2 \tag{46}$$

with

$$\mathbf{H} = \begin{bmatrix} \mathbf{A} & \frac{1}{2\sqrt{3}\Psi}\mathbf{A} \\ \frac{1}{2\sqrt{3}\Psi}\mathbf{A} & \frac{1}{\Psi^2}\mathbf{A} \end{bmatrix}, \quad \mathbf{A} = \begin{bmatrix} 1 & -0.5 & 0 \\ -0.5 & 1 & 0 \\ 0 & 0 & 3 \end{bmatrix} \tag{47}$$

The plastic projection is obtained by radial recovery. Fracture is modeled by visibility method. Therefore, the link between adjacent particles are removed. We employ stress-based criterion and fracture is introduced once a certain maximum principal stress-value is exceeded at the stress-points. Commonly, this threshold is equal to the tensile strength of the material.

5. NUMERICAL EXAMPLE: FRACTURE OF CYLINDRICAL SHELL

Experimental studies of fracture of cylindrical thin shells due to gas explosion were done by [Cha04]. In their experiments, they attached a thin-walled cylindrical shell made of aluminium to a rigid detonation tube. The rigid detonation tube had a length of 1.52m and the cylindrical aluminium tube had length of 89.6cm. The inner radius of the aluminium tube is $r_i = 1.975cm$ and shell thickness is 0.089cm. The aluminium tube contained notches of different length. We consider two notch length: 2.54cm and 7.6cm that is subsequently called short notch and long notch. In the experiment, [Cha04] sealed up the upper end while the lower end of the device was closed. Then, combustible gas was introduced in the tubes and thermally ignited. The combustion quickly turned into detonation. Since this is very difficult to model in numerical simulation, we modelled the detonation by pressure-time history on the inner walls of the cylinder that was also provided by [Cha04].

We now discuss results for short notch: At the beginning of the simulation, the crack extends from the two existing crack tips in a straight line in axial direction of the tube. The crack moving away the rigid tube slows down and the crack moving towards the rigid tube turns direction. It begins propagating in combined axial/circumferential direction with turning angle of approximately 45 degrees. Then this turning crack turns again and continues propagating only in circumferential direction. Simultaneously, crack growth at the opposite end is arrested. Final displaced configuration is illustrated in figure 3a and 3c. The displaced tube and failure pattern is similar to the experimental failure pattern.

We now discuss the results for long notch: First, crack starts propagating from two crack tips in straight line in axial direction. Then, both propagating cracks begin branching and change propagation direction mainly in circumferential direction. Several other small cracks at other location are nucleated that later join with the original main cracks. At the end of the simulation, the tube is split into three large pieces. The middle piece contains many smaller internal cracks. Also the tube in the experiment showed this behavior and was divided into 3 larger pieces where the middle piece contained internal cracks. The displaced tube at the end of the simulation is shown in figures 3b and 3d. It is shown next to the tube with short notch to emphasize the difference.

6. CONCLUSION

The fracture of thin-walled structures was studies with SPH shell formulation based on Mindlin Reissner theory. Therefore, the continuum SPH formulation was modified such that the behavior of the shell is determined using a model discretized only on mean surface alone. The mean surface consists of a single layer of particles in which

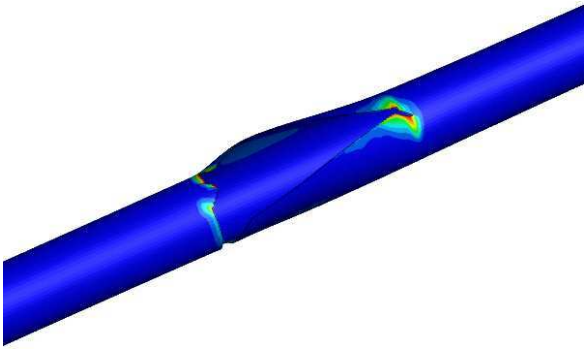

(a) short notch

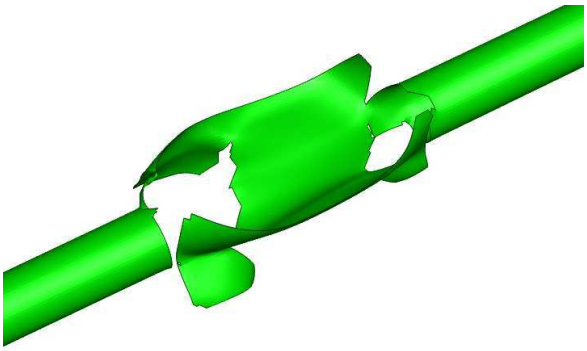

(b) long notch

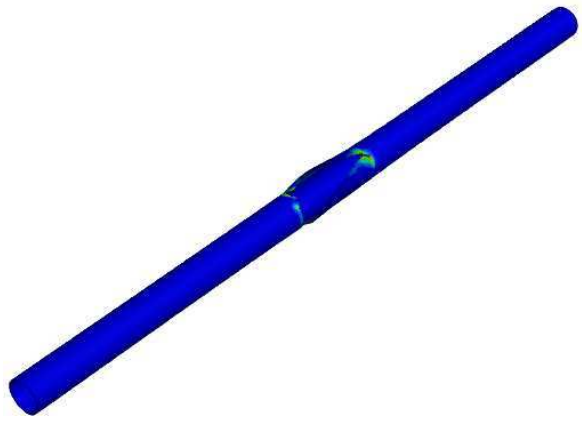

(c) short notch

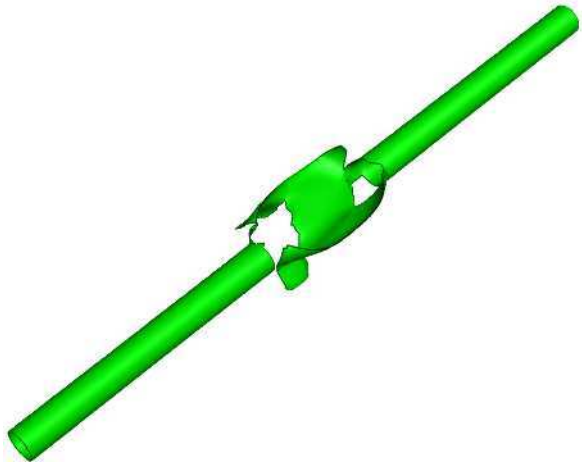

(d) long notch

Figure 3. Displaced configuration of cylindrical shell for short notch and long notch

each point on the mean plane is assigned a thickness that varies in space and time. Correction and stabilization of the classical SPH formulation is adopted from methods available in the literature. Moreover, elasto-plastic constitutive model is developed for the SPH shell and fracture criterion based on visibility method is used. The formulation is applicable to large deformations and finite rotation. The main contribution of this manuscript is a novel method for elasto-plastic fracture of thin walled structures. The major advantage over most existing formulations is computational efficiency.

We applied our method to two problems and compared results obtained from our numerical solution to experimental data. First example is tearing of plates with different notch-length. We did mesh refinement study and showed that results are independent of mesh. Agreement of our solution with experimental data are promising. The second more complex example is fracture of cylindrical shells due to a gas explosion. The gas explosion was modeled by pressure impulse on the inner walls of the cylinder according to experimental data. The cylindrical shells contained also pre-cracks of different length and failure mechanism depend on pre-crack length. When the notch is long, the tube broke into three large pieces while for short notch, the crack first propagates straight and then slightly curves. This behavior is also verified in our numerical model.

REFERENCES

[BK00] J. Bonet and S. Kulasegaram. Correction and stabilization of smooth particle hydrodynamics methods with application in metal forming simulations. *International Journal for Numerical Methods in Engineering*, 47(6):1189–1214, 2000.

[BKO+96] T. Belytschko, Y. Krongauz, D. Organ, M. Fleming, and P. Krysl. Meshless methods: An overview and recent developments. *Computer Methods in Applied Mechanics and Engineering*, 139:3–47, 1996.

[BLG95] T. Belytschko, Y.Y. Lu, and L. Gu. Crack propagation by element-free galerkin methods. *Engineering Fracture Mechanics*, 51(2):295–315, 1995.

[BT96] T. Belytschko and M. Tabbara. Dynamic fracture using element-free galerkin methods. *International Journal for Numerical Methods in Engineering*, 39(6):923–938, 1996.

[Cha04] TW Chao. Gaseous detonation-driven fracture of tubes. *PhD thesis, California Institute of Technology*, 2004.

[CWYY01] J-S Chen, C-T Wu, S Yoon, and Y.S. You. A stabilized conforming nodal integration for galerkin mesh-free method. *International Journal for Numerical Methods in Engineering*, 50:435466, 2001.

[FB07] J Feldman and J Bonet. Dynamic refinement and boundary contact forces in sph with applications in fluid flow problems. *International Journal for Numerical Methods in Engineering*, 72(3):295–324, 2007.

[GM77] RA Gingold and JJ Monaghan. Smoothed particle hydrodynamics: theory and application to non-spherical stars. *Monthly Notices of the Royal Astronomical Society*, 181:375–389, 1977.

[JB96] GR Johnson and SR Beissel. Normalized smoothing functions for sph impact computations. *Computer Methods in Applied Mechanics and Engineering*, 39:2127–2741, 1996.

[JVC04] M Javidruzi, A Vafai, and JF Chen. Vibration, buckling and dynamic stability of cracked cylindrical shells. *Thin-Walled Structures*, 42(1):79–99, 2004.

[KB96] P. Krysl and T. Belytschko. Analysis of thin shells by the element-free galerkin method. *International Journal for Numerical Methods in ENgineering*, 33:3057–3078, 1996.

[KB97] Y. Krongauz and T. Belytschko. Consistent pseudo derivatives in meshless methods. *Computer Methods in Applied Mechanics and Engineering*, 146:371–386, 1997.

[KHG08] A. Khayyer and S.D. Shao H. Gotoh. Corrected incompressible sph method for accurate water-surface tracking in breaking waves. *Coastal Engineering*, 55(3):236–250, 2008.

[LC04] KM Liew and XL Chen. Mesh-free radial point interpolation method for the buckling analysis of mindlin plates. *International Journal for Numerical Methods in Engineering*, 60:1961–1877, 2004.

[Lei01] VMA Leitao. A meshless method for kirchhoff plate bending problems. *International Journal for Numerical Methods in Engineering*, 52:1197–1130, 2001.

[LJZ95] W.K. Liu, S. Jun, and Y.F. Zhang. Reproducing kernel particle methods. *International Journal for Numerical Methods in Engineering*, 20:1081–1106, 1995.

[NKM00] H. Noguchi, T Kawashima, and T Miyamura. Element free analysis of shell and spatial structures. *International Journal for Numerical Methods in Engineering*, 47:1215–1240, 2000.

[OR99] MH Osman and TM Roberts. Prediction of the fatigue life of slender web plates using fracture mechanics concepts. *Thin-Walled Structures*, 35(2):81–100, 1999.

[RA06] T Rabczuk and P Areias. A meshfree thin shell for arbitrary evolving cracks based on an extrinsic basis. *Computer Modeling in Engineering & Sciences*, 16(2):115–130, 2006.

[RAB07] T Rabczuk, PMA Areias, and T Belytschko. A meshfree thin shell method for nonlinear dynamic fracture. *International Journal for Numerical Methods in Engineering*, 72(5):524–548, 2007.

[RB04] T. Rabczuk and T. Belytschko. Cracking particles: A simplified meshfree method for arbitrary evolving cracks. *International Journal for Numerical Methods in Engineering*, 61(13):2316–2343, 2004.

[RBX04] T. Rabczuk, T. Belytschko, and S.P. Xiao. Stable particle methods based on lagrangian kernels. *Computer Methods in Applied Mechanics and Engineering*, 193:1035–1063, 2004.

[RL97] P.W. Randles and L.D. Libersky. Recent improvements in sph modeling of hypervelocity impact. *International Journal of Impact Engineering*, 20:525–532, 1997.

[RL00] PW Randles and L Libersky. Normalized sph with stress points. *International Journal for Numerical Methods in Engineering*, 48:1445–1461, 2000.

[RPB05] M Rodriguez-Paz and J Bonet. A corrected smooth particle hydrodynamics formulation of the shallow-water equations. *Computers & Structures*, 83(17-18):1396–1410, 2005.

[SHA95] JW Swegle, DL Hicks, and SW Attaway. Smoothed particle hydrodynamics stability analysis. *Journal of Computational Physics*, 116:123134, 1995.

[VCL00] R Vignjevic, J Campbell, and LD Libersky. A treatment of zero-energy modes in the smoothed particle hydrodynamics method. *Computer Methods in Applied Mechanics and Engineering*, 184:6785, 2000.

[VE99] A Vafai and HE Estekanchi. A parametric finite element study of cracked plates and shells. *Thin-Walled Structures*, 33(3):211–229, 1999.

[VE06] A Vaziri and HE Estekanchi. Buckling of cracked cylindrical thin shells under combined internal pressure and axial compression. *Thin-Walled Structures*, 44(2):141–151, 2006.

[WC06] DD Wang and JS Chen. A locking-free meshfree curved beam formulation with the stabilized conforming nodal integration. *Computational Mechanics*, 39(1):83–90, 2006.